The inversion of spectral ratio H/V in a layered system using the Diffuse Field Assumption (DFA)

José Piña-Flores[1.2], Mathieu Perton[2], Antonio García-Jerez[3.4], Enrique Carmona[4], Francisco Luzón[3], Juan C. Molina-Villegas[5], and Francisco J. Sánchez-Sesma[2]

1-Instituto de Geofísica, Universidad Nacional Autónoma de México; C.U., Coyoacán 04510 D.F.; México. Emails: ead2009@hotmail.com;

2-Instituto de Ingeniería, Universidad Nacional Autónoma de México; C.U., Coyoacán 04510 D.F.; México. Emails: mathieu.perton@gmail.com; sesma@unam.mx

3-Departamento de Química y Física, Universidad de Almería. 04120 Almería, Spain. Emails: agarcia-jerez@ual.es, fluzon@ual.es

4-Instituto Andaluz de Geofísica. Universidad de Granada. C/ Profesor Clavera, 12. 18071 Granada, Spain. Email: ecarmona@ugr.es

5-Departamento de Ingeniería Civil, Universidad EAFIT, Medellín, Colombia. Email: jcmovi@gmail.com

Keywords: Site effects, Seismic noise, Wave Propagation, Joint inversion

Abstract

In order to evaluate the site effects on seismic ground motion and establish preventive measures to mitigate these effects, the dynamic characterization of sites is mandatory. Among the various geophysical tools aimed to this end, the horizontal to vertical spectral ratio (H/V) is a simple way to assess the dominant frequency of a site from seismic ambient noise. The aim of this communication is contributing to enhance the potential of this measurement with a novel method that allows extracting from the H/V the elastic properties of the subsoil, assumed here as a multilayer medium. For that purpose, we adopt the Diffuse Field Assumption from both the experimental and the modeling perspectives. At the experimental end, the idea is to define general criteria that make the data processing closely supported by theory. On the modeling front, the challenge is to compute efficiently the imaginary part of Green's function. The Cauchy's residue theory in the horizontal wavenumber complex plane is the selected approach. This method allows both identifying the contributions of body and surface waves and computing them separately. This permits exploring the theoretical properties of the H/V under different compositions of the seismic ambient noise. This answers some questions that historically aroused and gives new insights into the H/V method. The efficient forward calculation is the prime ingredient of an inversion scheme based on both gradient and heuristic searches. The availability of efficient forward calculation of *H/V* allows exploring some relevant relationships between the H/V curves and the parameters. This allows generating useful criteria to speed up inversion. As in many inverse problems, the non-uniqueness issues also emerge here. A joint inversion method that considers also the dispersion curves of surface waves extracted from seismic ambient noise is presented and applied to experimental data. This joint scheme mitigates effectively the non-uniqueness.

1. Introduction

The effects of surface geology can generate large ground motion amplification during earthquakes. The increase of amplitude and duration of seismic shaking can produce loss of lives and severe damage to infrastructure. The adequate assessment of local site effects is mandatory to establish preventive measures. In many cases, the amplification can be estimated using methods that simulate wave propagation in layered media, considering one-dimensional (1-D) variation of their properties (e.g. Thompson-Haskell). However, these methods require the mechanical properties of the stratigraphy as input, and this information can be costly.

Geophysical methods can provide an economic alternative to estimate dynamic site characteristics. Within these procedures, the horizontal to vertical spectral ratio (called HVSR or H/V) is quite popular, because it is a simple way to estimate the dominant frequency induced by local stratigraphy from both microtremor (ambient noise) or earthquake measurements (see Nakamura 1989; Bard 1999). However, this method has been controversial due to the absence of sound theoretical basis. In fact, many studies attempted to establish its strengths and limitations (Lermo & Chávez-García 1993; Lachet & Bard 1994; Mucciarelli 1998; Arai & Tokimatsu 2004; Guéguen *et al.* 2007; Cara *et al.* 2010). For example, it is not evident which waves compose the noise field at the H/V peak frequencies (Nakamura 2000; Malischewsky & Scherbaum 2004; Bonnefoy-Claudet *et al.* 2008).

Three main physical interpretations of the H/V spectral ratio have, so far been

proposed. They emerged from different points of view. In the first one, the predominant peak is related to the ellipticity of Rayleigh waves around the fundamental frequency of the site (Nogoshi & Igarashi 1971; Field & Jacob 1995; Horike 1996; Konno & Ohmachi 1998; Lachet & Bard 1994; Tokimatsu 1995) when there is a significant impedance contrast between the soil and the bedrock (Bard 1999). The second interpretation is due to Nakamura (1989; 2000), who suggests that the ratio H/V is related to the transfer function for vertical incidence of SH waves; the success of the H/V measurements was spectacular but it came along with controversy about the interpretation of the resulting spectral ratios. On the other hand, Sánchez-Sesma *et al*. (2010; 2011a) have proposed recently that microtremors form a Diffuse Field containing all types of body (*P* and *S*) and surface waves (Love and Rayleigh).

In a recent review, Lunedei and Malischewsky (2015) made a detailed description of the various theoretical models for the H/V spectral ratio developed in the last three decades. They identify two main research lines: ones attempt to describe the H/V curve by taking into account the complete seismic ambient-vibration wave field. The other line just studies the Rayleigh wave ellipticity. Regarding the first research line, there are two models of the ambient seismic wave field: the Distributed Surface Sources (*DSS*) model (Albarello & Lunedei 2011; Lunedei & Albarello 2015) and the Diffuse Field Assumption (*DFA*) (Sánchez-Sesma *et al.* 2011a). These models were compared recently (García-Jerez *et al.* 2011; 2012) and it was found that they provide similar results; particularly regarding the surface-wave behavior. The *DSS* is dependent on the source distribution. On the other hand, the *DFA* relies on a Diffuse Field illumination enhanced by multiple scattering. The *DFA* has strong theoretical links with deterministic problems (Sánchez-Sesma *et al.* 2011b). Lunedei and Malischewsky (2015) suggest that further investigations are required to clarify the differences between *DFA* and *DSS*.

Within the *DFA* it is assumed that the relative power of each seismic state that composes the illumination emerges from the Principle of Equipartition of Energy. Theory asserts that within a diffuse elastic wavefield the autocorrelation in frequency domain, at any point of the medium, is proportional to the imaginary part of the Green's function for coinciding source and receiver (Sánchez-Sesma *et al.* 2011a).

In this research we explore the properties of the H/V from a modeling perspective. Therefore, a fast numerical method to obtain the H/V for a horizontally layered medium is described. The keys of their efficiency are detailed. The method allows identifying the different parts of the elastic wave fields (body and/or surface waves) that contribute to the H/V. It is particularly useful to explore some properties of the H/V for several geological settings and different ambient noise compositions. In this context, to assess the soil elastic parameters from surface measurements, an inverse problem emerges. Several methods (of gradient and heuristic types) are useful for this purpose, and they all have advantages and limitations. Here we used both types depending upon the preliminary information that might be available. The non-uniqueness issues, inherent in any inversion process, can be mitigated performing joint inversion of H/V and dispersion curves.

The focus of this communication is the inverse problem, trying to give perspective for practical applications. We applied this approach to interpret data gathered in Almería (Spain) including joint inversion. A computer code, based on this formulation is described elsewhere (García-Jerez *et al*. 2016).

2. Theoretical H/V

It has been established that if the H/V is defined as the square root of the ratio between the horizontal and the vertical energies of a Diffuse Field, it is then possible to express this ratio in terms of the imaginary components of the Green function (Sánchez-Sesma *et al.* 2011a). In what follows, we summarize the arguments.

The Green's function can be retrieved from the average cross correlations of the displacements within the diffuse field because they are proportional:

$$\langle u_i(\boldsymbol{x_A},\omega)u_j^*(\boldsymbol{x_B},\omega)\rangle \propto \mathrm{Im}\big[G_{ij}(\boldsymbol{x_B},\boldsymbol{x_A};\omega)\big], \tag{1}$$

where $\omega = 2\pi f$ is the angular frequency, $u_i(\boldsymbol{x_A},\omega)$ is the displacement field component in i direction at point $\boldsymbol{x_A}$, $G_{ij}(\boldsymbol{x_B},\boldsymbol{x_A};\omega)$ is the Green's function defined as the displacement in direction i at point $\boldsymbol{x_B}$ due to the application of a unit harmonic point force in direction j applied at point $\boldsymbol{x_A}$. The asterisk $(*)$ means complex conjugation and the product in frequency domain (of one quantity and a complex conjugate) corresponds to the correlation operation in time domain.

If both source and receiver coincide, and the components are the same, the autocorrelation average corresponds to the directional energy density $E_i(\boldsymbol{x},\omega)$ at point $\boldsymbol{x}$ (Sánchez-Sesma *et al.* 2008; Perton *et al.* 2009):

$$E_i(\boldsymbol{x},\omega) = \rho\omega^2\langle\|u_i(\boldsymbol{x},\omega)\|^2\rangle \propto \mathrm{Im}[G_{ii}(\boldsymbol{x},\boldsymbol{x};\omega)], \tag{2}$$

where ρ is the mass density. On the other hand, following Arai & Tokimatsu (2004) we have:

$$H/V(\boldsymbol{x},\omega) = \sqrt{\frac{\langle\|u_1(\boldsymbol{x},\omega)\|^2\rangle + \langle\|u_2(\boldsymbol{x},\omega)\|^2\rangle}{\langle\|u_3(\boldsymbol{x},\omega)\|^2\rangle}} \tag{3}$$

where the subscripts 1 and 2 represent the horizontal directions while the subscript 3 corresponds to the vertical one. The ratio H/V can be experimentally computed in frequency domain in terms of the auto-correlations of the displacement signals from Eq. (3). For a diffuse wavefield, this equation can be expressed in term of the imaginary part of the Green's function components:

$$\mathrm{H/V}(\boldsymbol{x},\omega) = \sqrt{\frac{\mathrm{Im}[G_{11}(\boldsymbol{x},\boldsymbol{x};\omega)] + \mathrm{Im}[G_{22}(\boldsymbol{x},\boldsymbol{x};\omega)]}{\mathrm{Im}[G_{33}(\boldsymbol{x},\boldsymbol{x};\omega)]}}. \tag{4}$$

Eq. (4) gives the way to compute theoretically the H/V spectral ratio. In this expression, the Green's function components are associated to a specific geometry and to certain material properties. In this work, a layered halfspace with horizontal, unbounded interfaces is considered. The top surface is a free surface. The media are assumed homogeneous, isotropic and elastic with P and S waves velocities α and β, mass densities ρ and thickness h).

Our implementation of the Green's function retrieval neglects damping. It is known

that material properties can be strongly modified by viscosity. However, numerical experiments for Green's function retrieval show that for small damping its influence is moderate (Perez-Ruiz et al, 2008). In fact, the average cross-correlations do not match exactly the tensor Green's function, but the level of misfits is very low. This is in agreement with the results by Snieder et al. (2007) that the Green function can be retrieved from the response to random forcing for a variety of conditions, including the extreme case of the diffusion equation. Other experiments based on simple models with high impedance contrasts (e.g. Sánchez-Sesma et al., 2011a; Salinas et al., 2014; Sánchez-Sesma, 2016) allow to say that the main effect of anelastic attenuation is the decreasing of the main peak amplitude as the quality factor decreases, whereas the effects are almost negligible at higher frequencies, at which the Green's functions are dominated by surface waves.

The imaginary parts of the Green function, for a given frequency, can be expressed as integrals in the horizontal (radial) wavenumber domain and can be evaluated numerically (see Sánchez-Sesma *et al*. 2011a). One possible approach is to apply Bouchon's (2007) Discrete Wavenumber Method, instead the focus of this research is to isolate the contributions of the various waves. To this end, the expressions obtained by García-Jerez *et al*. (2013; 2016) are used. The kernels in the (k, ω) domain, where k = horizontal (radial) component of the wave vector, are extended to the complex k-plane. Since surface waves correspond to simple poles along the real-k axis, their contributions to the integrals are computed using the Cauchy's residue theorem. Branch cuts are introduced to establish appropriate integration contours (Tamura 1996). Moreover, body wave contributions are obtained by numerical integration along k in the finite interval $\left[0, +\frac{\omega}{\beta_N}\right]$, where β_N is the shear velocity of the half-space. As shown in García-Jerez *et al*. (2013; 2016) the expressions of the imaginary part of the Green's function, for the special case when source and receiver coincide at the top of the layered media, can be written in a very compact form. It is clear that the contributions from surface and body waves can be isolated:

$$\begin{aligned}\mathrm{Im}[G_{11}(0,0;\omega)] &= \mathrm{Im}[G_{22}(0,0;\omega)] \\ &= \underbrace{-\frac{1}{4}\left(\overbrace{\sum_m \chi_m^2 A_{Rm}}^{Rayleigh} + \overbrace{\sum_m A_{Lm}}^{Love}\right)}_{Surface\ waves} \\ &+ \underbrace{\frac{1}{4\pi}\int_0^{\omega/\beta_N} Re\left[f_{PSV}^H(k) + f_{SH}(k)\right]_{4^{th}}\,\mathrm{d}k}_{Body\ waves}, \end{aligned} \tag{5}$$

$$\mathrm{Im}[G_{33}(0,0;\omega)] = \underbrace{-\frac{1}{2}\left(\overbrace{\sum_m A_{Rm}}^{Rayleigh}\right)}_{Surface\ waves} + \underbrace{\frac{1}{2\pi}\int_0^{\omega/\beta_N} Re[f_{PSV}^V(k)]_{4^{th}}\,\mathrm{d}k}_{Body\ waves},$$

where $f_{PSV}^H(k)$, $f_{PSV}^V(k)$, $f_{SH}(k)$ are the kernels associated to the body waves in 3-D; χ_m is the ellipticity of the *collimated* m^{th} Rayleigh mode, and A_{Rm} and A_{Lm} correspond to

the medium responses for the m^{th} Rayleigh and Love modes, respectively (Harkrider 1964). The analytical computation of χ_m, A_{Rm} and A_{Lm} requires the precise location of the poles along the real *k*-axis. These positions are evaluated rapidly as they correspond to points of the dispersion curves at a given frequency (see *e.g.* García-Jerez *et al.* 2016). Even for a fine discretization the poles are likely to be lost and the computed integrals be wrong. To visualize the situation, a very small imaginary constant is added to frequency and this shifts the poles away from the real *k*-axis, just enough to plot the integrands. Figure 1 depicts the integrand of ImG_{33} at a complex frequency $f = (10 - i0.1)$ Hz for the stratigraphy given in Model 1 (Table 1).

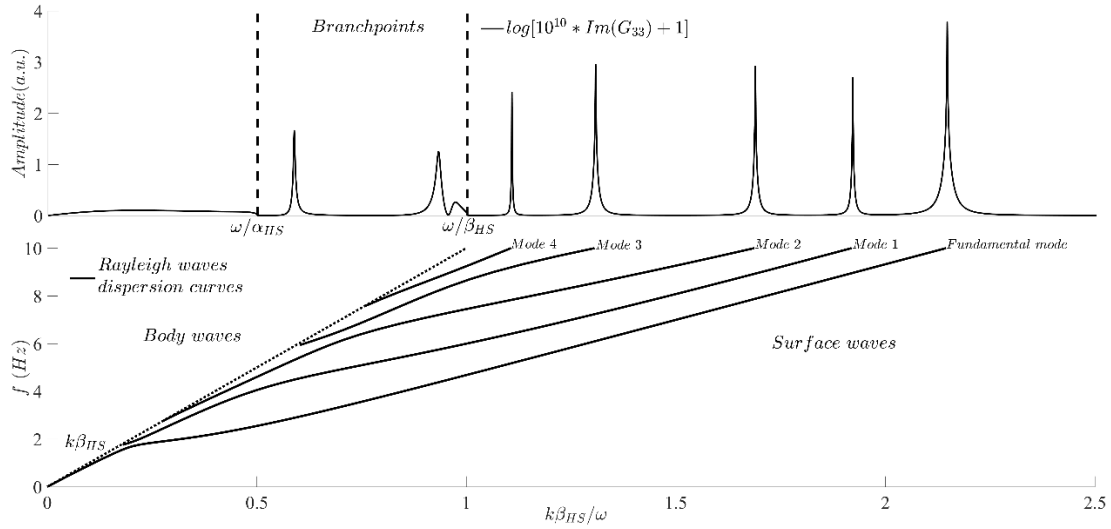

Figure 1: Top: integrand of the imaginary part of the Green's function component $\boldsymbol{G_{33}}$ at $\boldsymbol{f_{max}} = (\boldsymbol{10 - i0.1})$ Hz. Bottom: Rayleigh dispersion curves in plane $(\boldsymbol{k}, \boldsymbol{\omega})$, and limit $\boldsymbol{\omega = k\beta_{HS}}$. Only Rayleigh waves appear in $\boldsymbol{G_{33}}$. The limit corresponds to the separation between the parts containing either body or surface waves in the integrand. Here, we considered the model 1 (see Table 1). The positions of the poles in the integrand of the Green's function are given by the dispersion curves. The amplitude is compressed using the formula indicated in the legend.

Table 1. Example models used in this work.

h (m)	α(m/s)	β(m/s)	ρ(kg/m^3)
Model 1			
120	1000	500	1000
∞	2000	1000	3000
Model 2			
20	2100	500	1500
900	2138	1000	2000
∞	4330	2000	2500
Model 3			
20	1658	500	1200
100	2081	1000	1400
500	3970	2000	1500
1700	6062	3500	1700
∞	10950	6000	2800

3. Experimental H/V

The Diffuse Field Assumption (*DFA*) from the experimental perspective requires adopting general criteria that make the results of data treatment closely related to theory. We notice that the original H/V spectral ratio computations emerged from ideas close to transfer and receiver functions. It was then natural to see H/V as the average of individual ratios for a set of time windows. This was theoretically appealing because the spectral ratio "removes the source" in each time window and preserves the relative interactions of waves. While for receiver functions, this is advantageous for de-convolving the phases and find the structure, the large variability of H/V among the windows reveals also great variability of the sources and averaging is required.

In this work, we explore the *DFA* and the resulting average energy densities. The relationship of average directional energy densities with Green's function leaves the source issue open and resting upon the averaging process.

The Principle of Equipartition of Energy establishes that all modes will contribute with the same energy to build up the Green's function. Such set of modes constitute a Diffuse Field. In fact, some spectacular connections between analytical, deterministic solutions emerge from Diffuse Field theory (see Sánchez-Sesma *et al.* 2011b, Pérez-Ruiz *et al.* 2008, Perton and Sánchez-Sesma 2016).

Nature tends to equilibrate and the multiple scattering appears to be the mechanism producing the condition of equipartition of energy. We assume equipartition of illumination and/or multiple scattering lead to a diffusive wave regime. This allows connecting the average directional energy densities with Green's functions. Then a theoretical formula for H/V emerged from the DFA.

However, Nature produces more rich schemes; some can be identified. Early, in a pioneering study for 1-D problem, Claerbout (1968) established the relationship between energy density and Green's function. This fact was explicitly pointed out by Kawase et al. (2011) in their successful study of H/V for earthquake data having little or no surface waves. The theoretical H/V that explained data has only the contribution of body waves.

The approach presented herein allows to account separately the contributions of the various kinds of waves that form the field. They appear explicitly in formulae (5) and can be selected as desired to obtain theoretical H/V *a la carte* in order to identify the wave types that are effectively in the data (see Rivet *et al*. 2015).

In a recent research, Lin *et al.* (2012) processed teleseismic events recorded by the USArray and inverted jointly the ellipticity and the phase velocity of the Rayleigh wave fundamental mode to resolve the uppermost crustal structure. Significant research at longer periods is due to Lin *et al.* (2014). They did extended observations of ellipticity and confirmed their findings for shorter periods using ambient noise cross-correlations. These ellipticity measurements were interpreted in terms of 3D structure.

In another recent paper on the subject, Shen and Ritzwoller (2016) successfully constructed a new model of the shear velocity structure of the crust and uppermost mantle beneath the contiguous U.S. using data from more than a decade of USArray recordings. They performed a joint inversion of Rayleigh wave group and phase speeds determined from ambient noise and earthquakes, receiver functions, and measurements of Rayleigh wave ellipticity.

On the other hand, Mulargia (2012) claimed that the seismic noise is not diffuse. Despite this, he recognizes that seismic ambient noise may hold imaging properties. In the meantime, we assume that ambient seismic noise is diffusive and explore the

consequences.

Diffuse Field Theory rests on the DFA and that may produce meaningful results. All models, to a certain extent, are false; some are useful. For instance, the DFA lead to values of H/V that are *intrinsic properties* of the system. These should be compared with data adequately processed. A theory is a philosophy, a model, a scheme, an idea that produce results to be tested against reality. In this communication, we explore the main features of H/V under the DFA. The applicability issue of DFA was dealt with in Kawase et al (2015). They compared the results of Arai and Tokimatsu (2004) with the DFA calculations with excellent agreement. Inspired in the theory we normalize all the time windows in order to make them to have the same energy distributed in the three components. We believe that adequate data processing may enhance the diffuse properties of any noise field. This is a subject that requires further scrutiny.

4. Inversion of H/V

Having a theoretical estimate of H/V in terms of the Green's functions of system, it is natural to seek a contact with reality comparing with measured values and attempt inversion. The theoretical H/V depends on the layered system that has properties that emerge from the material elastic parameters and layers thicknesses. The blind inversion can be quite costly because it may imply a huge search within the parameter space and the convergence can require long time or even not be reached.

In order to sharpen the search of solutions, it is convenient to define upper and lower limits of target values, using *a priori* information (e.g. borehole, geology and geophysics data) or analyzing the shape of the experimental H/V itself. Its features may guide the inversion by using simplified models that mimic the observations. Therefore, a preliminary inversion based upon simple parametric analysis may be cost-effective in the inversion procedure.

Our theoretical model for simulation of H/V assumes that the layers are horizontal and unbounded. This geometrical configuration allows a fast calculation of the Green's functions and it is well suited for inversion.

The recommended method for the inversion of H/V curves depends on the existing constraints. When either no information or little *a priori* information is available, heuristic procedures such as the Simulated Annealing method should be considered (Goffe 1996, Goffe *et al.* 1994, Hastings 1970, Holland 1975, Kirkpatrick *et al.* 1983, Iglesias 2001). Its main advantage is the possibility to explore an extended parameter space, which may present several local minima, and to converge toward an optimum model. This method has already been successfully employed in seismology to invert the fundamental Rayleigh mode dispersion curves (Martínez *et al*. 2000; Iglesias *et al.* 2001; Beaty *et al*. 2002; Xia *et al.* 2002; Pei *et al*. 2007) and H/V (Spica *et al.* 2015; García-Jerez *et al.* 2016). When the misfit is already close to an acceptable value, or when enough *a priori* information is available, the inversion can be made using a local optimization scheme (e.g. Byrd *et al*. 1999, Waltz *et al.* 2006).

The misfit between model and observations should be minimized in any inversion process. In this work, we assume the cost-function or misfit Γ_{HV} defined as:

$$\Gamma_{HV} = \sum_{i=1}^{n} \frac{\left(HV_{obs}(\omega_i) - HV_{th}(\omega_i)\right)^2}{{\sigma_{HV}}^2(\omega_i)}, \qquad (6)$$

where HV_{obs} and HV_{th} correspond respectively to the experimental (target) measurements (or the reference model listed above) and the calculated H/V for the current trial model at the n chosen frequencies ω_i. σ_{HV} is the standard deviation resulting from the experimental computation of HV_{obs}.

If it is not available, it is replaced by a percentage of $\mathrm{H/V_{obs}}$ in order to make the cost function equally sensitive to relative errors.

The forward problem is non-linear and depends on several uncorrelated parameters (Piña-Flores 2015). Moreover, it is clear that several sets of parameters can be associated to the same H/V. For example, in figure 2, two velocity profiles give rise to the same H/V curve, demonstrating the non-uniqueness of the H/V inversion.

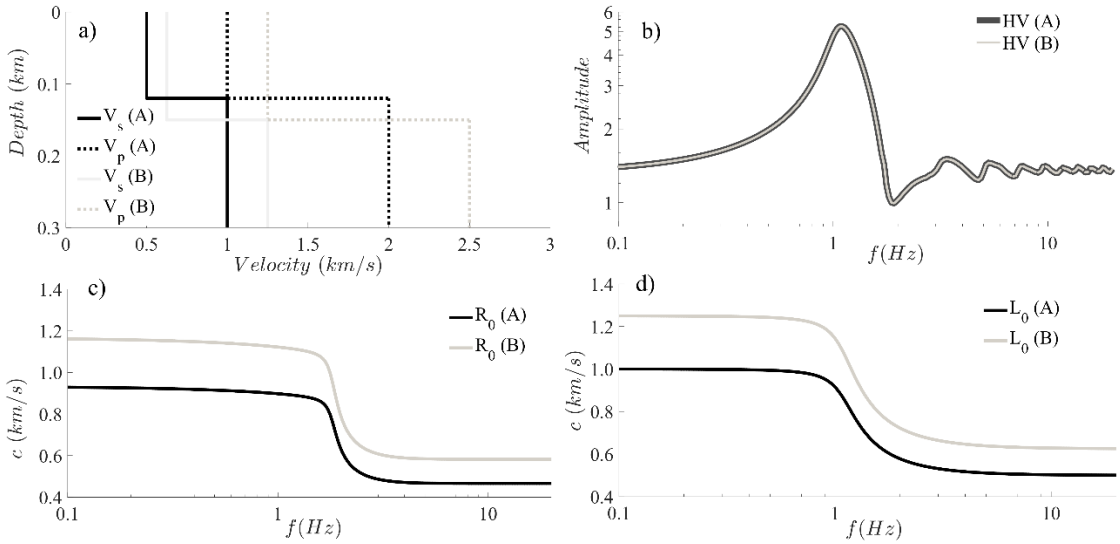

Figure 2: a) Two layered media profiles where A is the model 1 (see Table 1) and their associated b) H/V, c) Rayleigh and d) Love fundamental mode dispersion curves. These configurations show the non-uniqueness of the H/V inversion but this can be overcome when considering the joint inversion of H/V ratios and the dispersion curves of Love and/or Rayleigh fundamental modes.

This example of non-uniqueness was pointed out by Piña-Flores (2015) for the Rayleigh and Love dispersion curve. The cost function is depicted in figure 3 in terms of the shear velocities. The black band in figure 3-a is associated with global minima.

5. Inversion of H/V using supplementary information

Because of the non-uniqueness of the solutions associated to the single H/V inversion, using complementary information is highly recommended. This section explores two types of supplementary information that may allow defining bounds in the search space: The dispersion curves for both Love and Rayleigh surface waves and the parametric analysis of H/V. Scherbaum *et al.* (2003) suggested combining the H/V spectral ratio and the dispersion curve in a joint inversion, however, this approach was limited by the model used for the interpretation of the H/V spectral ratio.

5.1 Dispersion Curve

Since dispersion curves (DC) are computed at the same time of the theoretical H/V, the joint inversion of the fundamental Love and Rayleigh modes has no additional computational cost. To account jointly for all the information that both the H/V and the *DC* supply the cost function is adapted accordingly:

$$\Gamma = \frac{2(1-\xi)}{n}\sum_{i=1}^{n}\frac{\left(HV_{obs}(\omega_i) - HV_{th}(\omega_i)\right)^2}{{\sigma_{HV}}^2(\omega_i)} + \frac{2\xi}{m}\sum_{i=1}^{m}\frac{\left(DC_{obs}(\omega_i) - DC_{th}(\omega_i)\right)^2}{{\sigma_{DC}}^2(\omega_i)}, \qquad (7)$$

where $\xi = n/(n+m)$. If the number of data for both observables is the same, the cost function does not change. By taking terminology from Pei (2007), the Eq. (7) is called "equalized cost function". DC_{obs} and DC_{th} correspond, respectively, to the experimental measurement (target) and the calculated dispersion curve for the current trial model associated to the fundamental mode and evaluated at the m chosen frequencies ω_i. The confidence interval σ_{DC} results from the computation of the dispersion curves. Again, if it is not available, it can be replaced by a percentage of the target DC_{obs} in order to make the cost function equally sensitive to relative errors in the velocities.

As shown in figure 3-b, the DC may enable to distinguish the true solution from false ones. In this manner, the quantity of local minima is drastically reduced and the cost function is made smoother, which help the algorithms to converge more quickly to the true solution. The gradient method is then preferred in the joint inversion.

The single inversion of the DC associated to the fundamental mode of Rayleigh or Love waves presents the same difficulty as for the single inversion of the H/V, i. e. non-uniqueness of the problem and non-smooth cost function. In many experiments where DCs are measured with tri-axial sensors, there is almost no cost to calculate the H/V. The joint inversion of the DC and the H/V under this full-wavefield theory is therefore a promising seismic exploration method. Note that the DCs are sensible to the velocity structures while the H/V carries information associated to the travel times. Thus, these two kinds of information are then not redundant. The DCs can somehow be hard to obtain since they require good synchronization of the seismic stations, identification of modes and, eventually, the evaluation of travel path between the seismic stations. When using the SPAC technique for computation of DC, we implicitly assume that the surrounding stratigraphy is an average.

5.2 Parametric analysis

For a given configuration, a parametric analysis allows to get general indicators of trends in the model response. These indicators give clues that may help the inversion process. For instance, the values of frequencies associated to spectral peaks are strongly dependent on layers velocities and thicknesses.

The theoretical foundation of the H/V ratio for a diffuse wavefield allows discussing some of its properties and exploring new ones. For this purpose, three stratigraphic models are proposed in order to cover a wide range of configurations. They are described in Table 1.

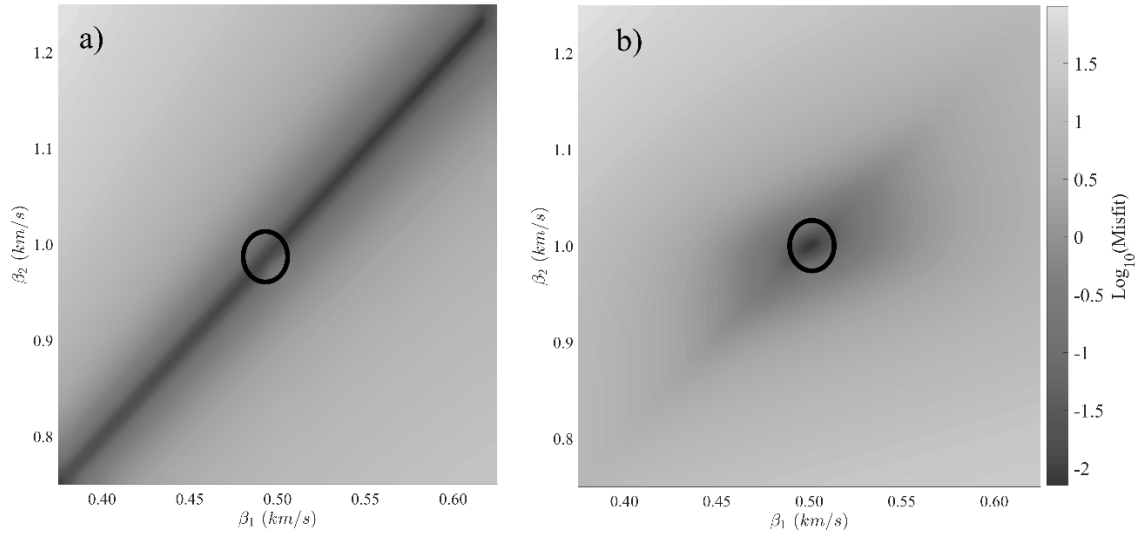

Figure 3: Cost surfaces associated to (a) H/V cost function given by Eq. (6) and (b) to the joint H/V and fundamental-mode Rayleigh-wave cost function given by Eq. (7). The cost surfaces are given as function of the shear velocities of the two layers, but the thicknesses and the P-wave velocities vary linearly with the shear velocities of the associated layers for the reference model 1 indicated with black circles (see Table 1).

Firstly, the separate contributions to the ratio H/V coming from the several types of waves that exist in a layered media are presented in figure 4-a for model 2 (see Table 1). By considering the contribution of the Rayleigh-wave fundamental mode only (dot-dashed line in figure 4-a), the H/V corresponds to the Rayleigh wave ellipticity (e.g. Lin et al 2012). This quantity was first studied as a simple proxy for the spectral ratio by Nogoshi & Igarashi (1971). Here, the shear impedance contrast between the two first layers equals 0.5, giving rise to a smooth ellipticity curve. However, when the contrast increases by varying the shear velocity of the first layer, the high frequency peak of the ellipticity is drastically amplified and the subsequent minimum decreases, but in this especial case, the ellipticity presents two minima (see figure 5). Generally, these high amplitude peaks correspond to minima of the vertical power spectrum V (see figure 4-b). This analysis was made by Konno & Ohmachi (1998). When considering the contribution of all the surface waves (black dashed line), oscillations appear at high frequencies and the overall amplitude of the spectral ratio increases in comparison with the previous case (see figure 4-a). When the diffuse field is dominated by body waves, as it is the case of the codas of deep earthquakes in Japan, the H/V ratio presents clear resonances at high frequencies (Kawase *et al*. 2011). In fact, the H/V ratio considering only the body waves contributions (see figure 4-a) is very similar to the transfer function for vertical *S* waves, in partial agreement with Nakamura's (1989) interpretation. Finally, when all the wave types are considered (Spica et al. 2015; Rivet et al. 2015 García-Jerez et al. 2016), the H/V ratio is usually dominated by surface wave contributions for frequencies higher than the first maximum, whereas it is dominated by body waves below that frequency (see figure 4-a) .

The frequency associated to the fundamental peak (generally the maximum amplitude of the H/V) is usually employed to roughly determine the thickness of the layer (one layer over half-space model), when its shear velocity is known or vice versa, by means of the simple formula $f_{\beta_1} = \frac{\beta_1}{4h_1}$ where h_1 and $\beta_1$are the thickness and shear

velocity for the layer. The accuracy of this formula is represented in figure 6 using model 1 (Table 1) with variable β_1. It results that the approximation is very good for this case, since the maximum error remains as low as 5% over all the Poisson's ratio range [0.05, 0.49]. García-Jerez *et al*. (2012) studied the dependence between the β_1 contrast and the fundamental frequency. For low contrasts, the frequency of the peak shifts toward low frequencies. The frequency associated to the first minimum that follows the first peak can also be employed to estimate the thickness of the first layer, when its compressional velocity is known, by using the simple formula $f_{\alpha_1} = \frac{\alpha_1}{4h_1}$, where h_1, α_1 are the thickness and compressional velocity for the superficial layer. The accuracy of this formula is presented in figure 7 using model 1 (Table 1) with variable α_1. In this case, the error is high in the Poisson's ratio range [0.34, 0.49], but the approximation offers a maximum error of 10% in the Poisson's ratio range [0.05, 0.34]. When two layers are considered on top of a half space, the H/V can present at most two peaks depending on the thickness of each layer and the velocity and mass density contrasts. If the thickness of the deep layer is greater than the surface layer and a sufficient impedance contrast between these three materials exists, the two main peaks are well separated. For example, we can consider the H/V ratio for model 2 (Table 1), shown in figure 8. The two main peaks can be defined as those having large amplitudes as compared to the surface wave oscillations (visible as wiggles in-between the peaks) and should not be mistaken with these ones. In this case, provided that $\beta_2 \gg \beta_1$ and $h_2 \gg h_1$, the shear velocity of the superficial layer can also be evaluated using the formula $f_{\beta_1} = \frac{\beta_1}{4h_1}$, where f_{β_1} represents the high frequency peak. Moreover, the approximate frequency associated to the peak at low frequencies can be evaluated from $f_{\beta_{12}} = \frac{1}{4\left(\frac{h_1}{\beta_1}+\frac{h_2}{\beta_2}\right)}$, where h_2 and β_2 are the thickness and shear velocity for the second layer. The accuracy of this formula is displayed for model 2 in figure 9. The approximation is very good since it provides a maximum error of 10% over the Poisson's ratio range [0.2, 0.49].

Recently, Tuan et al. (2015) developed an approximate explicit equation for the peak frequency of H/V ratio for multilayered models with high impedance contrast between the half-space and surface layers. This formula was generalized for a model of graded material layer over a half-space. Later, Tuan et al. (2016) obtained an explicit exact expression from the response of vertically incident SH Waves. This formula reflects several major effects of the model on the resonance frequency such as the arrangement of layers and the impedance contrast. They show that for large average impedance contrast the peak frequencies from the improved formula and the peaks of H/V under DFA are consistent.

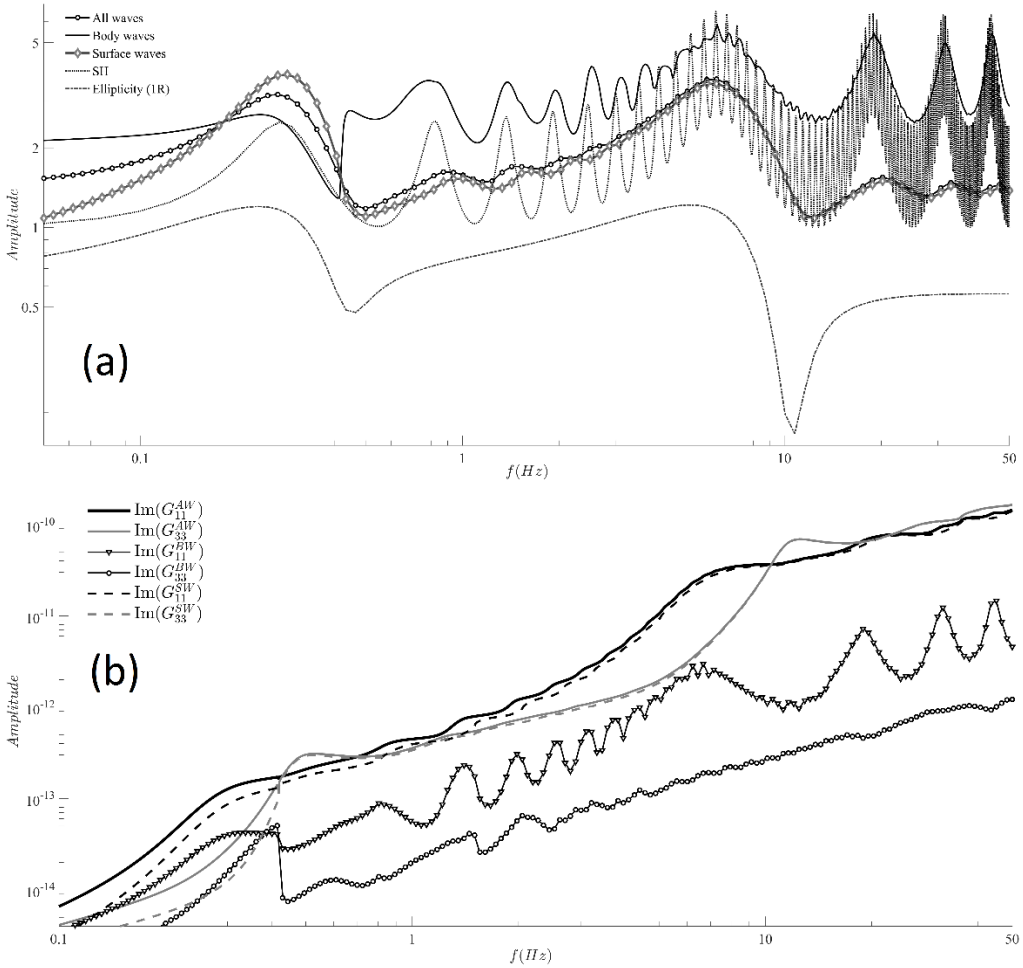

Figure 4: a) H/V calculated by considering different types of waves for model 2 (Table 1): fundamental Rayleigh mode (open circles line), all the surface wave modes (open triangle line), body waves (dot line) and all the surface modes and the body waves (diamond line). The transfer function *SH* (solid line) is very similar to the H/V ratio computed for body wave's contributions. b) Im[G_{11}], Im[G_{33}] and contributions of body and surface waves to these quantities.

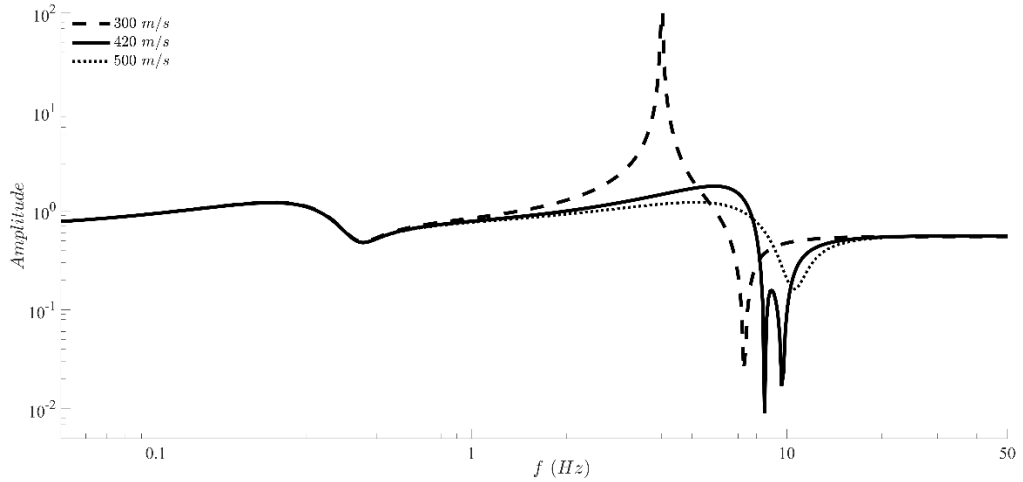

Figure 5: H/V spectral ratio considering the fundamental Rayleigh mode (ellipticity) only. Dotted line corresponds to model 2 (Table 1) . Solid and dashed lines are generated by varying the shear velocity of the first layer.

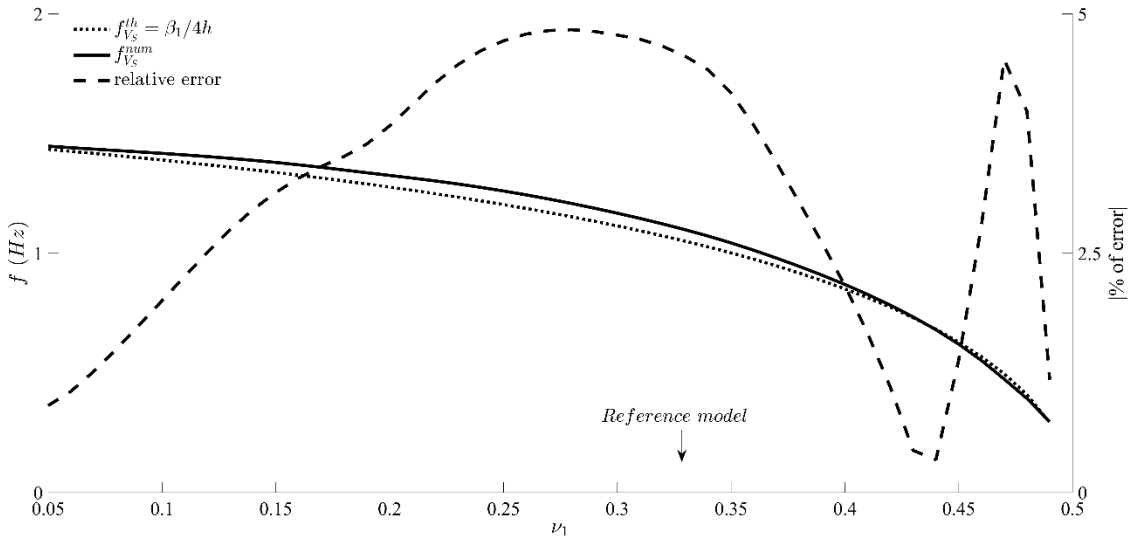

Figure 6: Frequency associated to the main peak in the H/V ratio considering illumination made up of all the waves types, measured from simulations (solid line) and from the simple formula $\boldsymbol{f_{\beta_1} = \frac{\beta_1}{4h_1}}$ (dotted line). The frequencies are plotted as a function of the Poisson's ratio of the first layer for model 1 (Table 1). Only the shear velocity $\boldsymbol{\beta_1}$ of the first layer has been varied. The relative error on the approximation is also given in percentage (dashed line).

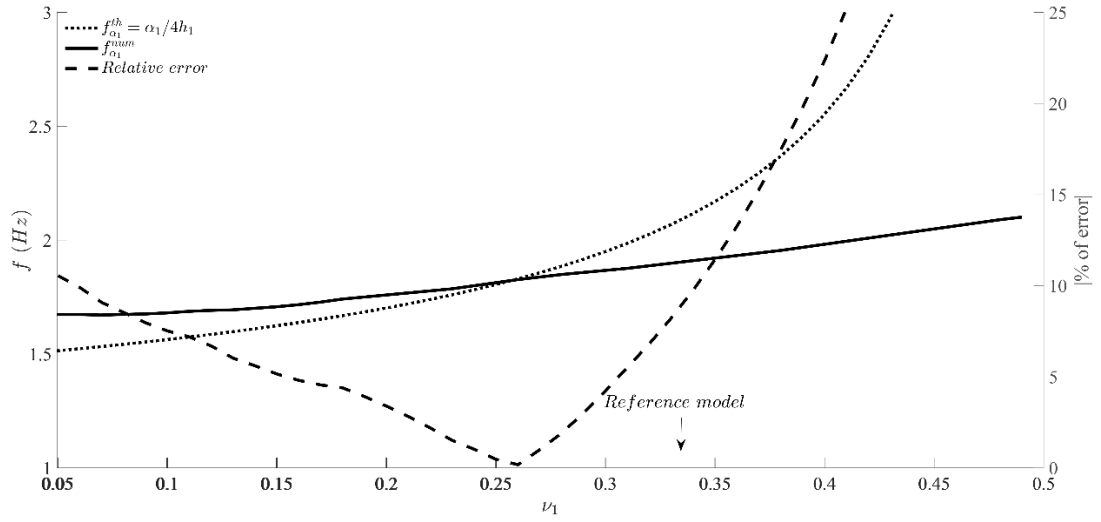

Figure 7: Solid line shows the frequency of the first minimum in H/V measured from simulations which take all types of waves into account. The result of the simple formula $\boldsymbol{f_{\alpha_1} = \frac{\alpha_1}{4h_1}}$ is shown with a dotted line. The frequencies are plotted as a function of the Poisson's ratio of the first layer, varying the velocity $\boldsymbol{\alpha_1}$ in model 1 (Table 1). The relative error in the approximation is given in percentage (dashed line).

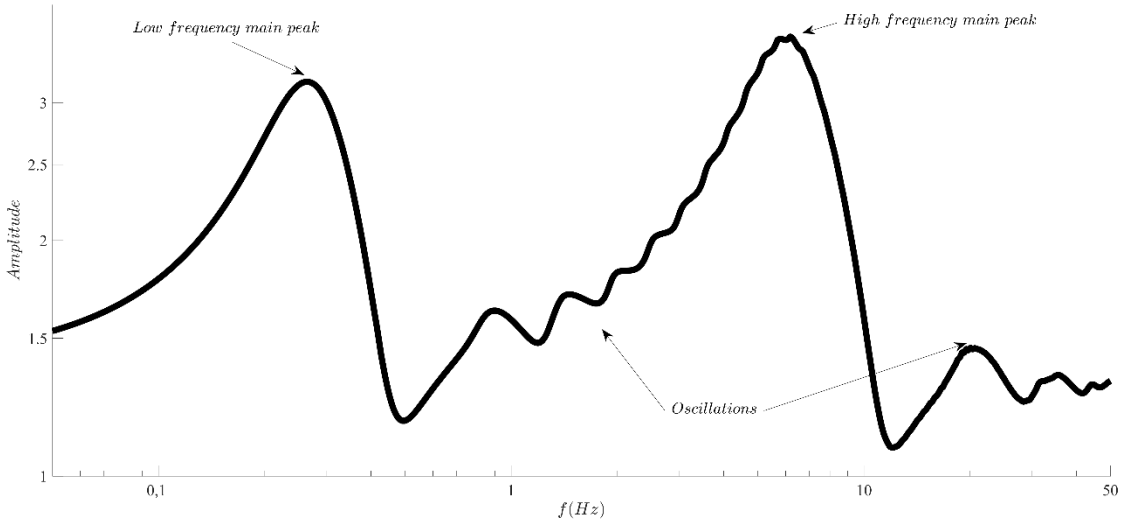

Figure 8: H/V for model 2 (Table 1). Two main peaks are well separated and some oscillations due to the surface and body waves in the horizontal component are visible in-between.

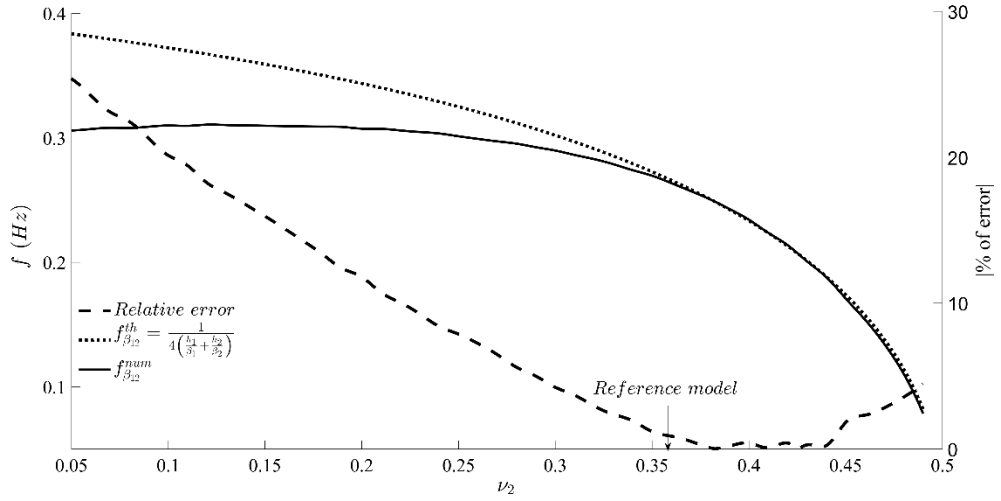

Figure 9: Frequency associated to the low frequency peak of the H/V ratio (see figure 8) considering the illumination from all waves for model 2, measured from simulations (solid line) and from the simple formula $\boldsymbol{f_{\beta_{12}} = \frac{1}{4\left(\frac{h_1}{\beta_1}+\frac{h_2}{\beta_2}\right)}}$ (dotted line). The frequencies are plotted in function of the Poisson's ratio of the second layer. Only the shear velocity of the second layer has been varied. The relative error on the approximation is also given in percentage (dashed line).

In general, it is suggested that the minimum number of layers to consider for an H/V inversion can be equal to the number of main peaks. For example, four main peaks are observed in figure 10, which has been obtained by considering model 3 (Table 1).

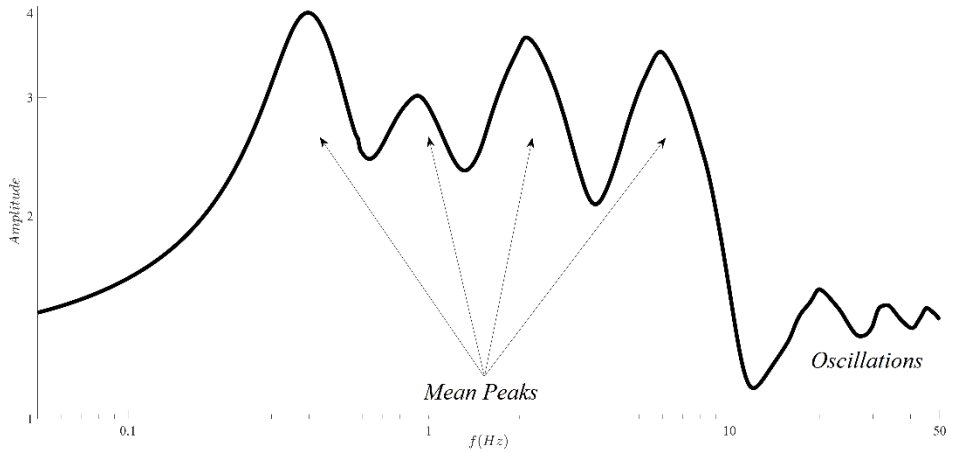

Figure 10: H/V computed by considering the model 3 (Table 1). The number of main peaks, those that appear below 10 Hz, indicates the minimum number of layers that should be considered in the inversion.

6. Application to the Almería zone (Spain)

The joint-inversion method has been applied to the Bajo Andarax river area (SE Spain), where the accumulation of sedimentary material may lead to significant site effects. This area includes a part of Almería city, with about 200,000 inhabitants. Two measurements were carried out in the sites indicated in the figure 11. Here we use data form a single station (*ER20*) located close to the experimental seismic array deployment. The Rayleigh wave DC was obtained at this site in previous studies (García-Jerez 2010a) using the *SPAC* technique with five concentric pentagonal setups of radius 12, 18, 25, 50, 94, and 420 m, without a central station. The ambient noise recordings were measured continuously for 1 hour. The time windows considered for correlation were 40s long with 50% overlapping.

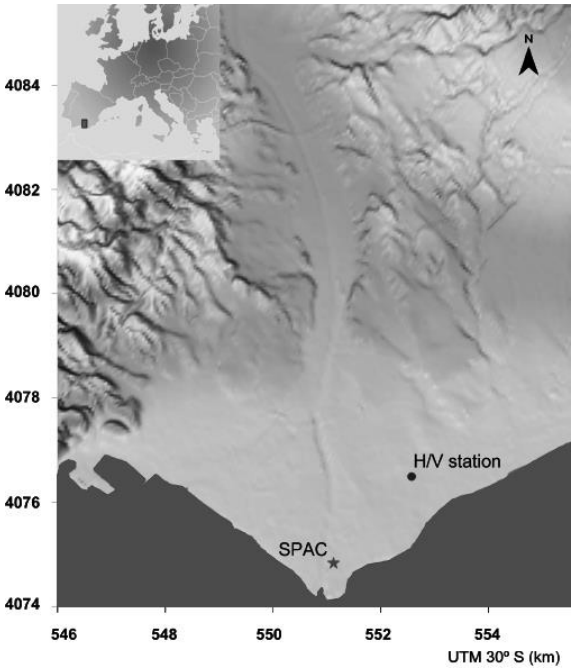

Figure 11: Location of the H/V and *SPAC* measurements. (UTM coordinates).

The target H/V curve obtained using data from ambient noise (see Figure 12-a) has three main peaks at frequencies 0.38, 2.5 and 6.2 Hz. As was shown in Section 5.2, the number of main peaks is an indicator of minimum number of layers on the half-space (see Figure 8). However, a layer may have intercalated materials, which together can give as a whole a similar response as that of a single layer (Piña-Flores 2015). Another important feature of the target H/V curve is the presence of oscillations between the major peaks of 0.38 and 2.5 Hz. (see Figure 12-a). This indicates that there are relatively large thicknesses of the deeper layers (see Figure 8).

The amplitude of the major peaks in the target H/V curve, are indicators of significant changes between wave velocities and/or densities between the layers (see Piña-Flores 2015). One of the advantages of having dispersion curve data, in addition to joint inversion, lies in the possibility to obtain the apparent velocities associated with the uppermost layers. All these indicators of the target H/V curve allow defining search ranges that ease and speed the inversion process for found the best solution.

Figure 12 shows the inversion for this location. A shear wave velocity model obtained with a different seismic method for a nearby location is shown in Fig. 12 panel c (García-Jerez et al. 2010). The depth of the basement agrees well with the results of independent geophysical studies carried out in the ‘80s by the Spanish Geological Survey (IGME 1983). The fundamental Rayleigh mode associated to the profiles shown in figure 12c is very close to the experimental one. The agreement in H/V is also very good in the frequency range common with the dispersion curve. Below 0.7 Hz, the agreement is fair and some uncertainties on the depth of the profile remain. The manifestation of these uncertainties is visible on the gray curves associated to current preliminary (or transition) inversion results with an error less than two times the final error. Since three main peaks are visible on the H/V here, a profile with three layers on top on a half-space has been considered.

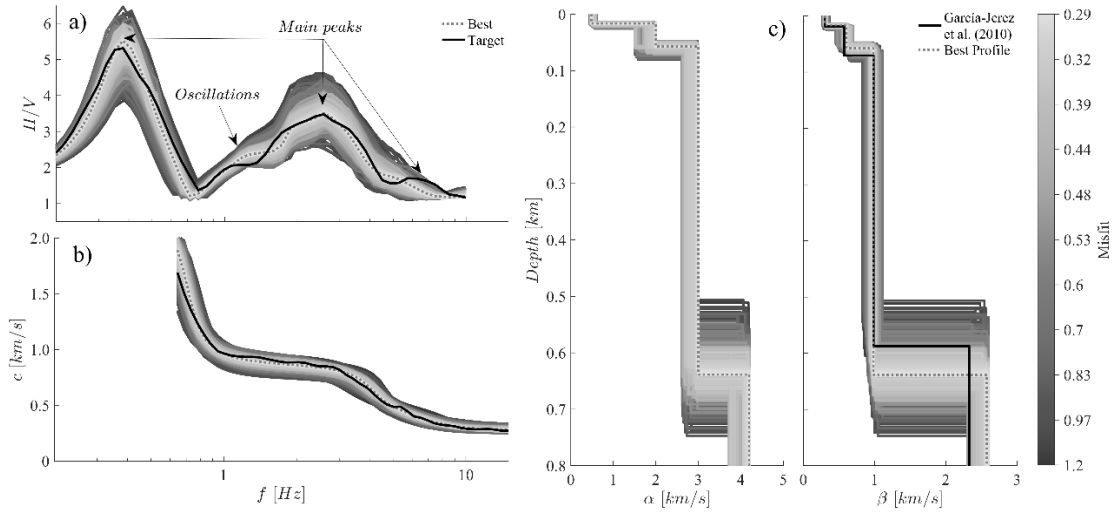

Figure 12: Results of the inversion for one of the locations at the mouth of Bajo Andarax river. a) H/V target and theoretical H/V for the best-fitting model. b) Rayleigh fundamental mode target and theoretical dispersion curve for the best fitting model. c) Velocity profile, the gray curves are associated to trial model generated by the iterative method with misfits less than two times the final error. The depth of bedrock is about 0.65 km and agrees well with geophysical prospecting developed in the early ‘80s by the Spanish Geological Survey (IGME 1983). Solid line represents a $\boldsymbol{\beta(z)}$ model obtained for a nearby site with a seismic method (García-Jerez *et al.* 2010b).

Tokimatsu et al. (1992) and Lunedei and Albarello (2016) have stressed the need to distinguish between effective and modal dispersion curves (DC) because in practice the energy transport can be accomplished by a multi modal trade-off. This topic requires additional research along their ideas.

7. Conclusions

The Diffuse Field Assumption allows obtaining reliable estimates of the H/V spectral ratio as an *intrinsic* property of a given uniform layered profile in terms of the imaginary components of the Green's function. Such calculation can be very fast by using the classical Cauchy's residue theorem. Moreover, this scheme allows the retrieval of the various wave types contributing to the H/V. In this way, the various contributions of body and surface waves within the Green's function can be isolated for further analysis. The fast calculation of H/V spectral ratio allowed the efficient inversion of the site layered structure using heuristic schemes such as the Simulated Annealing method when little or no *a priori* information is available, or by local techniques when the misfit is close to an acceptable value, or when some information is already available. Moreover, the theoretical H/V computations allow the parametrical exploration of the most conspicuous properties of this curve and are helpful to understand subtle effects due to variations of the elastic parameters.

The non-uniqueness of the solutions associated to the single H/V inversion is reduced drastically without additional computational cost by considering jointly the inversion of H/V and dispersion curves. The joint-inversion experiment for the Bajo Andarax river mouth area (Almería, Spain) is a clear example of the goodness of this approach.

Acknowledgements

Thanks are given to M. H. Ritzwoller, D. Albarello and an anonymous reviewer for their constructive comments and keen remarks. We also thank G. Sánchez, E. Plata and their team of the Unidad de Servicios de Información (USI) of the Institute of Engineering-UNAM for locating useful references. This study has been partially supported by the Spanish Ministry of Economy and Competitiveness under grant CGL2014-59908/JIN, by the EU with FEDER and by AXA Research Fund and by DGAPA-UNAM under Project IN104712.

References

Albarello, D. & Lunedei, E. (2011), 'Structure of an ambient vibration wavefield in the frequency range of engineering interest ([0.5, 20] Hz): insights from numerical modeling', *Near Surface Geophysics* **9**(6), 543–559.

Arai, H. & Tokimatsu, K. (2004), 'S-wave velocity profiling by inversion of microtremor H/V spectrum', *Bulletin of the Seismological Society of America* **94**(1), 53–63.

Bard, P. Y. (1999), '*Microtremor measurements: a tool for site effect estimation?,* A.A. Balkema/Rotterdam/Brookfiel/1999.

Beaty, K., Schmitt, D. & Sacchi, M. (2002), 'Simulated annealing inversion of

multimode Rayleigh wave dispersion curves for geological structure', *Geophysical Journal International* **151**(2), 622–631

Bonnefoy-Claudet, S., Köhler, A., Cornou, C., Wathelet, M. & Bard, P. Y. (2008), 'Effects of Love waves on microtremor H/V ratio', *Bulletin of the Seismological Society of America* **98**(1), 288–300.

Bouchon, M. & Sánchez-Sesma, F.J., 2007. 'Boundary integral equations and boundary elements methods in elastodynamics'. *Advances in geophysics, 48*, pp.157-189.

Byrd, R. H., Hribar, M. E. & Nocedal, J. (1999), 'An interior point algorithm for large-scale nonlinear programming', *SIAM Journal on Optimization* **9**(4), 877–900.

Cara, F., Di Giulio, G., Milana, G., Bordoni, P., Haines, J. & Rovelli, A. (2010), 'On the stability and reproducibility of the horizontal-to-vertical spectral ratios on ambient noise: case study of Cavola, northern Italy', *Bulletin of the Seismological Society of America* **100**(3), 1263–1275.

Claerbout, J. F. (1968), 'Synthesis of a layered medium from its acoustic transmission response', *Geophysics* **33**(2), 264-269.

Field, E. H. & Jacob, K. H. (1995), 'A comparison and test of various site-response estimation techniques, including three that are not reference-site dependent', *Bulletin of the seismological society of America* **85**(4), 1127–1143.

García-Jerez, A. (2010a), 'Desarrollo y evaluación de métodos avanzados de exploración sísmica pasiva. Aplicación a estructuras geológicas locales del sur de España', PhD thesis in Spanish, Universidad de Almería, España.

García-Jerez, A., Luzón, F., Navarro, M. & Santoyo, M. A. (2010b) Assessing the reliability of the single circular array method for Love-wave ambient noise surveying. *Bulletin of the Seismological Society of America* **100**(5), 2230-2249.

García-Jerez, A., Luzón, F., Sánchez-Sesma, F., Santoyo, M., Albarello, D., Lunedei, E., Campillo, M. & Iturrarán-Viveros, U. (2011), 'Comparison between two methods for forward calculation of ambient noise H/V spectral ratios', *in* 'AGU Fall Meeting Abstracts', Vol. 1, p. 2230

García-Jerez, A., Luzón, F., Albarello, D., Lunedei, E., Santoyo, M., Margerin, L. & Sánchez-Sesma, F. (2012), 'Comparison between ambient vibrations H/V obtained from the diffuse field and the distributed surface sources models', *in* '15th World Conference on Earthquake Engineering, IAEE, Lisbon, Portugal', pp. 24–28.

García-Jerez, A., Luzón, F., Sánchez-Sesma, F. J., Lunedei, E., Albarello, D., Santoyo, M. A. & Almendros, J. (2013), 'Diffuse elastic wavefield within a simple crustal model. some consequences for low and high frequencies', *Journal of Geophysical Research: Solid Earth* **118**(10), 5577–5595-

García-Jerez, A., Piña-Flores, J., Sánchez-Sesma, F. J., Luzón, F. & Perton, M. (2016), 'A computer code for forward computation and inversion of the H/V spectral ratio under the diffuse field assumption', *Computers & Geosciences* 97, 67–78.

Goffe, W. L. (1996), 'Simann: A global optimization algorithm using simulated annealing', *Studies in Nonlinear Dynamics & Econometrics* **1**(3).

Goffe, W. L., Ferrier, G. D. & Rogers, J. (1994), 'Global optimization of statistical functions with simulated annealing', *Journal of Econometrics* **60**(1), 65–99.

Guéguen, P., Cornou, C., Garambois, S. & Banton, J. (2007), 'On the limitation of the H/V spectral ratio using seismic noise as an exploration tool: application to the Grenoble valley (France), a small apex ratio basin', *Pure and Applied Geophysics* **164**(1), 115–134.

Harkrider, D. G. (1964), 'Surface waves in multilayered elastic media I. Rayleigh and Love waves from buried sources in a multilayered elastic half-space', *Bulletin of the Seismological Society of America* **54**(2), 627–679.

Hastings, W. K. (1970), 'Monte Carlo sampling methods using Márkov chains and their applications', *Biometrika* **57**(1), 97–109.

Holland, J. H. (1975), 'Adaptation in natural and artificial systems', *Ann Arbor MI: The University of Michigan Press*.

Horike, M. (1996), 'Geophysical exploration using microtremor measurements', In Proceedings of the 11th World Conference on Earthquake Engineering, Acapulco, Mexico. 23-28 June 1996. Paper 2033.

Iglesias, A., Cruz-Atienza, V. M., Shapiro, N. M., Singh, S. K. & Pacheco, J. F. (2001), 'Crustal structure of south-central México estimated from the inversion of surface-wave dispersion curves using genetic and simulated annealing algorithms', *Geofísica Internacional* **40** (3), 181–190.

IGME (1983), '*Prospección geotérmica en la depresión de Almería*', Vol. V. Madrid, Spain. In Spanish. http://info.igme.es/ConsultaSID/presentacion.asp?Id=800

Kawase, H., Sánchez-Sesma, F. J. & Matsushima, S. (2011), 'The optimal use of horizontal-to-vertical spectral ratios of earthquake motions for velocity inversions based on diffuse-field theory for plane waves', *Bulletin of the Seismological Society of America* **101** (5), 2001–2014.

Kawase, H., Matsushima, S., Satoh, T. & Sánchez-Sesma, F. J. (2015), 'Applicability of Theoretical Horizontal-to-Vertical Ratio of Microtremors Based on the Diffuse Field Concept to Previously Observed Data' *Bulletin of the Seismological Society of America,* doi: 10.1785/0120150134.

Kirkpatrick, S., Gelatt, C. D. & Vecchi, M. P. (1983), 'Optimization by simulated annealing', *Science* **220**(4598), 671–680.

Konno, K. & Ohmachi, T. (1998), 'Ground-motion characteristics estimated from spectral ratio between horizontal and vertical components of microtremor', *Bulletin of the Seismological Society of America* **88**(1), 228–241.

Lachet, C. & Bard, P.-Y. (1994), 'Numerical and theoretical investigations on the possibilities and limitations of Nakamura's technique', *Journal of Physics of the Earth* **42**(5), 377–397.

Lin, F.-C., Schmandt, B. & Tsai,V. C. (2012), 'Joint inversion of Rayleigh wave phase velocity and ellipticity using USArray: Constraining velocity and density structure in the upper crust', *Geophysical Research Letters* **39** L12303 doi:10.1029/2012GL052196.

Lin, F.-C., Tsai, V.C., & Schmandt, B. (2014), '3-D crustal structure of the western United States: application of Rayleigh-wave ellipticity extracted from noise crosscorrelations', *Geophysical Journal International,* doi: 10.1093/GJI/ggu160.Lermo, J. & Chávez-García, F. J. (1993), 'Site effect evaluation using spectral ratios with only one station', *Bulletin of the Seismological Society of America* **83**(5), 1574–1594.

Lunedei, E. & Albarello, D. (2015), 'Horizontal-to-vertical spectral ratios from a full-wavefield model of ambient vibrations generated by a distribution of spatially correlated surface sources', *Geophysical Journal International* **201**(2), 1140–1153.

Lunedei, E. & Malischewsky, P. (2015), 'A review and some new issues on the theory of the H/V technique for ambient vibrations', *in* Perspectives on European

Earthquake Engineering and Seismology, Springer, pp. 371–394.
Lunedei, E. & Albarello, D. (2016), 'Power spectral density function and spatial autocorrelation of the ambient vibration full-wavefield generated by a distribution of spatially correlated surface sources', *Geophysical Journal International* 204 (3), 1817-1837.
Malischewsky, P. G. & Scherbaum, F. (2004), 'Love's formula and H/V-ratio (ellipticity) of Rayleigh waves', *Wave motion* **40**(1), 57–67.
Martínez, M., Lana, X., Olarte, J., Badal, J. & Canas, J. A. (2000), 'Inversion of Rayleigh wave phase and group velocities by simulated annealing', *Physics of the Earth and Planetary Interiors* **122**(1), 3–17.
Mucciarelli, M. (1998), 'Reliability and applicability of Nakamura's technique using microtremors: an experimental approach', *Journal of Earthquake Engineering* **2**(04), 625–638.
Mulargia, F. (2012), 'The seismic noise wavefield is not diffuse', *The Journal of the Acoustical Society of America* **131**, 2853–2858.
Nakamura, Y. (1989), 'A method for dynamic characteristics estimation of subsurface using microtremor on ground surface', *QR of RTRI* 30(1), 25-33
Nakamura, Y. (2000), 'Clear identification of fundamental idea of Nakamura's technique and its applications', *in* 'Proceedings of the 12th World Conference on Earthquake Engineering', Auckland New Zealand.
Nogoshi, M. & Igarashi, T. (1971), 'On the amplitude characteristics of microtremor (part 2)', *Journal Seismological Society of Japan* **24**, 26–40.
Pei. D. (2007): 'Modeling and inversion of dispersion curves of surface waves in shallow site investigations', PhD thesis, University of Nevada, Reno.
Pei, D., Louie, J. N. & Pullammanappallil, S. K. (2007), 'Application of simulated annealing inversion on high-frequency fundamental-mode Rayleigh wave dispersion curves', *Geophysics* **72**(5), R77–R85.
Pérez-Ruiz, J. A., Luzón, F. & Sánchez-Sesma, F. J. (2008), 'Retrieval of elastic Green's tensor near a cylindrical inhomogeneity from vector correlations', *Communications in Computational Physics* 3, 250-270.
Perton, M., Sánchez-Sesma, F. J., Rodríguez-Castellanos, A., Campillo, M. & Weaver, R. L. (2009), 'Two perspectives on equipartition in diffuse elastic fields in three dimensions', *Journal of the Acoustical Society of America* **126**, 1125–1130.
Perton, M. & Sánchez-Sesma, F.J. (2016) 'Green's function calculation from equipartition theorem', *Journal of the Acoustical Society of America* 140, 1309.
Piña-Flores, J. (2015), 'Cálculo e inversión del cociente H/V a partir de ruido ambiental'. MSc thesis, Instituto de Geofísica. Universidad Nacional Autónoma de México., México DF. In Spanish. Link: http://132.248.9.195/ptd2015/enero/303134174/Index.html.
Rivet, D., Campillo, M., Sánchez-Sesma, F. J., Shapiro, N. M. & Singh, S. K. (2015), 'Identification of surface wave higher modes using a methodology based on seismic noise and coda waves', *Geophysical Journal International* **203**(2), 856-868.
Salinas, V., Luzón, F., García-Jerez, A., Sánchez-Sesma, F.J., Kawase, H., Matsushima, S., Suarez, M., Cuellar, A. & Campillo, M. (2014), 'Using diffuse field theory to interpret the H/V spectral ratio from earthquake records in Cibeles seismic station, Mexico City'. *Bulletin of the Seismological Society of America* 104 (2), 995–1001.

Sánchez-Sesma, F. J., Pérez-Ruiz, J. A., Luzón, F., Campillo, M. & Rodríguez-Castellanos, A. (2008), 'Diffuse fields in dynamic elasticity', *Wave Motion* **45**, 641–654.

Sánchez-Sesma, F. J., Rodríguez, M., Iturrarán-Viveros, U., Rodríguez-Castellanos, A., Suárez, M., Santoyo, M. A., García-Jerez, A. & Luzón, F. (2010), 'Site effects assessment using seismic noise', *in* Proceedings of the 9th International Workshop on Seismic Microzoning and Risk Reduction, pp. 21–24.

Sánchez-Sesma, F. J., Rodríguez, M., Iturrarán-Viveros, U., Luzón, F., Campillo, M., Margerin, L., García-Jerez, A., Suárez, M., Santoyo, M. A. & Rodríguez-Castellanos, A. (2011a), 'A theory for microtremor H/V spectral ratio: application for a layered medium', *Geophysical Journal International* **186**(1), 221–225.

Sánchez-Sesma, F. J., Weaver, R. L., Kawase, H., Matsushima, S., Luzón, F. & Campillo, M. (2011b), 'Energy partitions among elastic waves for dynamic surface loads in a semi-infinite solid', *Bulletin of the Seismological Society of America* **101**(4), 1704–1709.

Sánchez-Sesma, F.J. (2016), 'Modeling and inversion of the microtremor H/V spectral ratio: physical basis behind the diffuse-field approach'. In: Proceedings 5th IASPEI / IAEE International Symposium: Effects of Surface Geology on Seismic Motion, Taipei, Taiwan, p. 1–8.

Scherbaum, F., Hinzen, K.-G. & Ohrnberger, M., 2003, 'Determination of shallow shear wave velocity profiles in the Cologne, Germany area using ambient vibrations', *Geophysical Journal International* **152**, 597-612.

Shen, W. & Ritzwoller, M.H., 2016, 'Crustal and uppermost mantle structure beneath the United States', *J. Geophys. Res. Solid Earth*, doi: 10.1002/2016JB012887.

Snieder R., K. Wapenaar & U. Wegler (2007). ‚Unified Green's function retrieval by cross-correlation; connection with energy principles', Phys. Rev. E, 75, 036103-1-14.

Spica, Z., Caudron, C., Perton, M., Lecocq, T., Camelbeeck, T., Legrand, D., Piña-Flores, J., Iglesias, A. & Syahbana, D. K. (2015), 'Velocity models and site effects at Kawah Ijen volcano and Ijen caldera (Indonesia) determined from ambient noise cross-correlations and directional energy density spectral ratios', *Journal of Volcanology and Geothermal Research* **302**, 173–189.

Tamura, S. (1996), 'Comparison of body and Rayleigh wave displacements generated by a vertical point force on a layered elastic medium', *in* Proc. 11th World Conf. Earthquake Engineering.

Tokimatsu, K., Tamura, S. & Kojima, H. (1992), 'Effects of multiple modes on Rayleigh wave dispersion characteristics', *Journal of Geotechnical Engineering* **118**(10), 1529–1543.

Tokimatsu, K. (1995). 'Geotechnical Site Characterization using Surface Waves'. *Proceedings First International Conference on Earthquake Geotechnical Engineering, IS-Tokyo '95*, Tokyo, November 14-16, Balkema, Rotterdam, 1333-1368.

Tuan, T. T., Vinh, P. C., Malischewsky, P. & Aoudia, A. (2015), 'Approximate formula of peak frequency of H/V ratio curve in multilayered model and its use in H/V ratio technique', *Pure and Applied Geophysics* **173**, 487-498.

Tuan, T. T., Vinh, P. C., Ohrnberger, M. Malischewsky, P. & Aoudia, A. (2016), 'An improved formula of fundamental resonance frequency of a layered half-space model used in H/V ratio technique', *Pure and Applied Geophysics.* doi 10.1007/s

00024-016-1313-0
Waltz, R. A., Morales, J. L., Nocedal, J. & Orban, D. (2006), ‘An interior algorithm for nonlinear optimization that combines line search and trust region steps’, *Mathematical Programming* **107**(3), 391–408.
Xia, J., Miller, R. D., Park, C. B. & Tian, G. (2002), ‘Determining *Q* of near-surface materials from Rayleigh waves’, *Journal of Applied Geophysics* **51**(2), 121–129.